HELIUM RELEASE IN A CLOSED ENCLOSURE: COMPARISONS BETWEEN SIMPLE MODELS, CFD CALCULATIONS AND EXPERIMENTAL RESULTS

G. Bernard-Michel[1] and B. Cariteau[2]

[1]*DRN/DMT/SEMT/LTMF, Bât. 454, CEA Saclay, Gif-Sur-Yvette, France, e-mail : gilles.bernard-michel@cea.fr*
[2]*DRN/DMT/SEMT/LEEF, Bât. 454, CEA Saclay, Gif-Sur-Yvette, France, e-mail : benjamin.cariteau@cea.fr*

ABSTRACT

In the prospect of a safe use of hydrogen in our society, one important task is to evaluate under which conditions the storage of hydrogen systems can reach a sufficient level of safety. One of the most important issues is the use of such system in closed area, for example a private garage or an industrial facility. In the scope of this paper, we are mainly interested in the following scenario: a relatively slow release of hydrogen (around 5Nl/min) in a closed and almost cubic box, representing either a fuel cell at normal scale, or a private garage at a smaller scale. For practical reasons, helium was used instead of hydrogen in the experiments on which are based our comparisons. This kind of situation leads to the fundamental problem of the dispersion of hydrogen due to a simple vertical source in an enclosure. Many numerical and experimental studies have already been conducted on this problem showing the formation of either a stably stratified distribution of concentration or the formation of a homogeneous layer due to high enough convective flows at the top of the enclosure. Nevertheless, most of them consider the cases of accidental situation in which the flow rate is relatively important (higher than 10Nl/min). Numerical simulations carried out with the CEA code Cast3M and a LES turbulence model confirm the differences of results already observed in experimental helium concentration measurments for a same injection flow rate and two different injection nozzle diameters, contradicting simple physical models used in safety calculations.

NOMENCLATURE

α	Helium concentration	μ	Viscosity [Pa.s]
μ_t	Turbulent viscosity [Pa.s]	ρ_{he}	Helium density [kg.m^{-3}]
ρ_a	Air density [kg.m^{-3}]	ρ	Mixture density [kg.m^{-3}]
σ	Schmidt number	C_s	Smagorinsky constant
d	Helium diffusivity to air [m^2.s^{-1}]	l_m	length of the convective jet [m]
Ri_0	Injection Richardson number	$\mathbf{g}$	Gravity acceleration vector [m.s^{-2}]
P	Pressure [Pa]	Q_{he}	Helium injection flow rate [m^3.s^{-1}]
$\mathbf{u}$	Mixture velocity [m.s^{-1}]	r	Radial coordinate [m]
r_i	Nozzle radius [m]	V_h	Cell surface [m^2]
z	vertical coordinate [m]		

I. INTRODUCTION

During the release of a buoyant fluid in an enclosure, concentration builds up. When the buoyant fluid is a potentially flammable gas mixture, this build-up might endanger the safety of the persons or of the materials in the surroundings. As hydrogen is expected to come into widespread use in the near future, this problem of the concentration distribution in enclosure finds a renewed interest.

The distribution of the buoyant gas in the enclosure depends on many parameters, among them: the release rate, momentum and buoyancy flux, the volume of the enclosure and the position of the source. Different typical regimes have already been identified. We consider our enclosure as closed since the experimental results are studied in a time range where interactions with the decompression hole are negligible. Without ventilation, we can find mainly two regimes depending on the ratio of the injected momentum to the potential energy required to mix the entire volume. If the injected momentum is high enough, the entire volume can be mixed resulting in a constant concentration over the space. If not, a vertical stratification takes place [3]. It is possible, for intermediate regimes, to find an homogeneous layer at the top of the enclosure, under which a stratification takes place down to the bottom. If we have a closer look at the phenomenon, the jet or plume impacts the ceiling and spreads toward the side walls after what a horizontal density front moves downward. Baines and Tuner [1] give an analytical description of the velocity of the first front and the final density profile once the front has reached the floor. Their model is extended by Worster and Hupper [2] to describe the time evolution of the vertical density profile during the first stage of descending front. In some cases, Cleaver, Marshall and Linden [3] show that the vertical density profile exhibits a well defined homogeneous layer near the ceiling under which the density increases linearly.

In these purposes, and more particularly in the scope of the project ANR PANH DIMITRHY, a set of experiments has been conducted on a small scale facility which dimensions are typical of a fuel cell, approximately 1 cubic meter [4]. Helium was used as a model gas of hydrogen. For small injection momentum (less than 5 Nl/min), strong differences were observed between concentrations with the 5mm diameter nozzle and the 20mm diameter nozzle. Helium concentration profiles obtained with the 20mm nozzle are similar to those given by the Worster and Hupper model [2], whereas concentrations measured with the 5mm nozzle are almost twice higher than predicted. The goal of this paper is to find an explanation to this differences with the help of numerical simulations, giving access to the velocity fields and turbulence levels.

The present paper is organised as follows. The experimental techniques are presented in section 2. Section 3 is devoted to the set up of numerical simulations: numerical scheme, mesh generation and turbulence model. Section 4 is dedicated to the results. Comparisons are made with experimental results. We conclude in section 5.

II. EXPERIMENTAL DESCRIPTION

We are simulating an experimental set-up: a parallelepiped enclosure with a square base of 0.93m wide and 1.26m high. One small vent of 10mm diameter is located 10mm from the floor at the middle of the back side. This vent is there to prevent the enclosure pressure to rise when the helium

jet is released, Figure 1. Helium concentrations are affected by the vent when - after a certain time - stratified or homogeneous layer reaches the bottom of the enclosure. This will be prenvented by selecting a limited enough time range in our study.

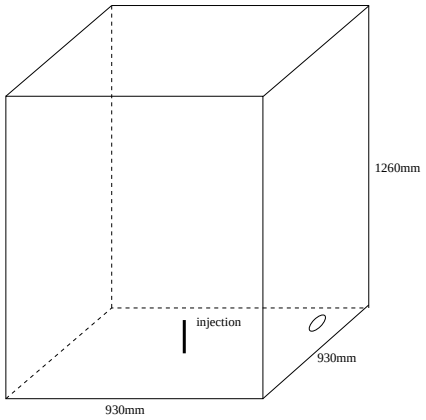

FIG. 1: Closed enclosure with a small aperture.

Local time variations of the volume fraction are measured by Mini-katharometers TCG-3880 from Xensor. From manufacturer fact the long term absolute error on the volume fraction measurement is about 0.07%. The sensors are located at five levels along two vertical lines (see Fig. 2). The enclosure is placed in a garage with insulated walls. Temperature variations are lower than 0.1 °C.

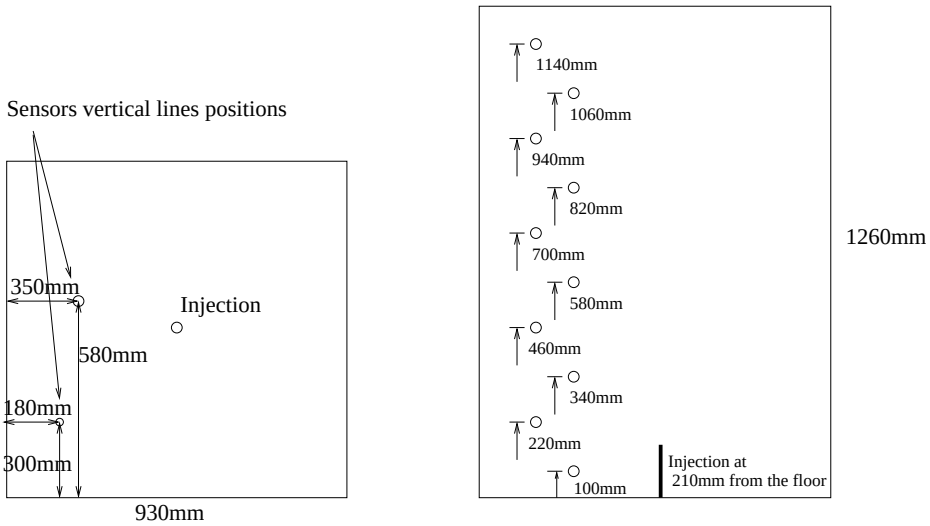

FIG. 2: Schematic representation of the experimental set-up with source and volume fraction measurement probes (cross) locations.

Helium is injected either through a 5mm or a 20 mm diameter vertical nozzle which exit is 210mm from the floor. The flow rate is controlled with mass flow regulators between. We are only focusing on results obtained for a flow rate of 4 Nl/min and 5 Nl/min, respectively with a 20 mm diameter nozzle and a 5 mm diameter nozzle. A summary of the experimental conditions is given in Table I. With the diameter D of the nozzle, the density ρ_a of the ambient and ρ_{he} of the helium injected,

the volume flow rate at the nozzle Q_{he} and the gravity acceleration g, the injection Richardson number is defined as (see e.g. [5]):

$$Ri_0 = \frac{\pi^2}{32}\frac{\rho_a - \rho_{he}}{\rho_{he}}\frac{gD^5}{Q_{he}^2} \quad (1)$$

Its order of magnitude for the selected flow rates varies from 0.01 (for 5 mm diameter injection nozzle) up to 3 (for the 20 mm diameter) which indicates that in the first case the flow is dominated by convection as the fluid exits the nozzle and that in the second case the flow is rapidly dominated by buoyancy as soon as the fluid exits the nozzle. We also introduce the average length of the jet at the injection nozzle, which indicates the transient distance ahead of which the jet becomes buoyant [6]: $l_m = 3Q_{he}/(S^{3/4}\sqrt{g'})$ where $g' = g(\rho_a - \rho_{he})/\rho_{he}$ is the reduced gravity and S is the injection surface of the nozzle. The length l_m varies from 0.03 **m** (for the 20 mm diameter nozzle) up to 0.3 **m** (for the 5 mm diameter), to be compared to the 1.26 m height of the enclosure.

TABLE I: Experimental conditions.

D (mm)	Q_{he} (Nl/min)	Ri_0	l_m (m)	T (°C)	injection time (s)
5	5	0.01	0.3	20.5	500
20	4	3	0.03	19.5	1200

III. GEOMETRICAL SIMPLIFICATIONS

Experimental results were showing one dimensional dependency of the helium volume concentration along the vertical axis [4]. Therefore it is not necessary to consider the original parallelepiped shape of the enclosure. We can simplify the geometry in our numerical simulations. We consider a cylinder of the same height and the same section as the original enclosure, see Figure 3.

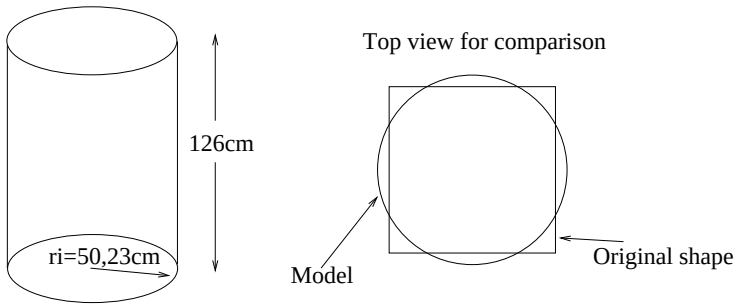

FIG. 3: Equivalent cylinder shape enclosure.

This geometry captures correctly the initial jet, which is mainly occupying the centre of the enclose. The concentration distribution being only dependant on the vertical position in the rest of the enclosure, the cross section's shape (circle or square) is not of important if the area is conserved. We make a second assumption, which on the other hand may degrade much more the quality of the simulations: we consider the flow is axisymmetrical around the jet injection axis. We know from BOSS visualisation of the concentration gradients in the experiments that the jet in not purely axisymmetrical [4], at least when it is purely buoyant, as in the 4 Nl/min injection case with a 20mm nozzle. Nevertheless, as we will see in the results section, this do not affect too much the quality of the simulations results.

IV. CONSERVATION EQUATIONS

The mixing of helium with air was calculated by solving the two dimensional axisymmetrical transient, incompressible conservation equations for mixture mass (continuity equation), mixture momentum with Boussinesq approximation (two velocities) and helium volume fraction:

Mixture mass conservation

$$\nabla.\mathbf{u} = 0, \tag{2}$$

where $\mathbf{u}$ is the mixture velocity.

Mixture momentum

$$\rho_a \frac{\partial \mathbf{u}}{\partial t} + \rho_a \nabla.\mathbf{u} \otimes \mathbf{u} = -\nabla P + \nabla.\left((\mu + \mu_t)\nabla \mathbf{u}\right) + \rho \mathbf{g}, \tag{3}$$

where P is the pressure of the mixture, μ, μ_t the laminar and the turbulent viscosity of the mixture and ρ the density of the mixture defined as $\rho = \alpha \rho_h e + (1-\alpha)\rho_a$, where α is the volume fraction of helium in the mixture.

Turbulent viscosity

$$\mu_t = C_s^2 V_h \sqrt{S_{ij} S_{ij}}, \tag{4}$$

Turbulence was modeled using a LES Smagorinsky model [7, 8] where $C_s = 0.2$ is the Smagorinsky constant, V_h is the surface of mesh where μ_t is evaluated, and S_{ij} the displacement tensor.

Helium volume fraction

$$\rho_{he} \frac{\partial \alpha}{\partial t} + \rho_{he} \nabla.\mathbf{u}\alpha = \nabla.\left((\rho_{he} d + \frac{\mu_t}{\sigma})\nabla \alpha\right), \tag{5}$$

The molecular diffusivity of helium to air is taken to be $d = 5.649410^{-5}\ \mathbf{m^2/s}$ as in [9], the turbulent Schmidt and Prandtl number $\sigma = 0.72$ and α is the helium volume concentration.

V. INITIAL AND BOUNDARY CONDITIONS

Initial conditions

Temperature remain constant and equal to $293.5\mathbf{K}$ for the 5mm diameter test case and equal to $292.5\mathbf{K}$ for the 20mm test case. Velocity and concentration are null at time zero.

Walls conditions

The velocity is set to 0 on each wall of the enclosure. The normal derivative of the helium volume fraction α is set to 0, ensuring no diffusive flux of helium across the walls.

Small aperture for depressurisation

For the tiny hole located close to the bottom of the enclosure, we consider the following condition: $\partial u_r/\partial r = 0$ where u_x is the radial velocity and r the radial coordinate. We impose $\alpha = 0$ on that boundary.

Injection surface

At the injection surface, we impose the following velocity profile :

$$u_z = \frac{f_r Q_{he}}{\pi r_i^2} \tag{6}$$

where r_i is the radius of the injection nozzle, z is the vertical coordinate and u_z is the vertical velocity. The radial velocity is set to 0 at the injection. This velocity profile ensures that for $\alpha = 1$ (pure helium at the injection), we obtain Q_{he} for the injected helium flux. Therefore, f_r is a parabolic function, whose integral along the injection surface is equal to 1: $f_r = \frac{1}{2}(r_i^2 - r^2)$.

For the helium volume concentration, we impose the total flux:

$$\rho_{he}\alpha u_z \ + \ (\rho_{he} d + \frac{\mu_t}{\sigma})\frac{\partial \alpha}{\partial z} = Q_{he} f_r \tag{7}$$

Axis of symmetry

On the axis, we impose null fluxes, that is $\partial\alpha/\partial r = 0$ and $u_r = 0$.

VI. GRID AND DISCRETIZATION

The mesh is unstructured, composed of triangles. We are using 7 nodes quadratic finite elements for the velocity and the volume fraction discretization. We are using 3 nodes linear finite elements for the pressure. These elements satisfy the LBB conditions [10].

The scheme is implicit with an algebraic double projection method for the coupled mixture mass and momentum equations [11]. The scheme is stable, convergent, with no CFL conditions. However, the projection method and the linearisation of the convective terms requires a fix point Picard algorithm [12] which requires the global matrix of the system to be lipschitz contractant. Practically, it requires small enough time steps for the internal iterations to converge. The convection scheme is centred. There is no upwind scheme or diffusion whatsoever added to the convective terms.

Mesh size

Two grids are produced: the first one for the 5mm case and the other one for the 20mm case. The strategy is to have a fine grid at the injection with at least 10 nodes on one injection radius, then along the axis, and at the top of the enclosure where a large vortex and 2 impacts with the top wall and the right wall are observed. At first we had used an adaptive automatic mesh refinement technique. It proved to be more economical for the 20mm case, but more difficult to use with the

5mm case where mesh size is ranging from 0.1mm up to a few centimetres. Finally, we have chosen two fixed grids, see Figure 4.

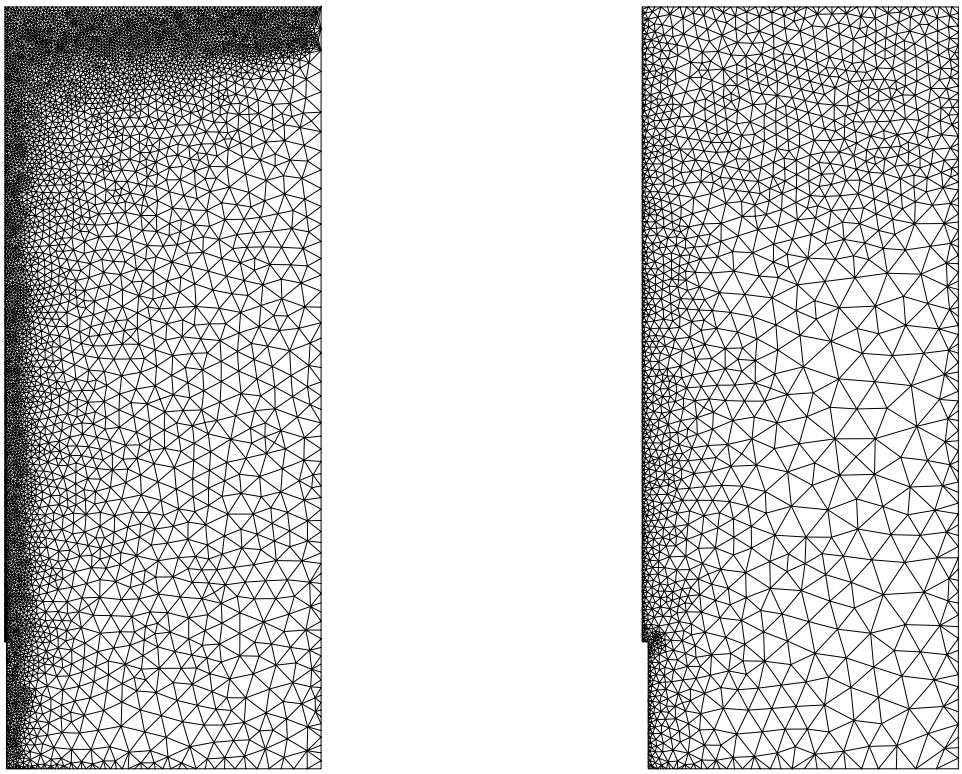

FIG. 4: The two grids used for the 5mm (left) and the 20mm (right) test cases.

We also summarise the main characteristics of the grids Table II.

TABLE II: The computational grids main characteristics.

Case	Number of nodes	Min cell size (mm)	Max cell size
1 (20mm)	2300	2.0	40
2 (5mm)	11700	0.5	20

Time steps

Time steps have been chosen constant. Simulations have been achieved with different times steps until no variations were observed (less than 1 %). The time variation discretization is an implicit BDF2 scheme [12]. Although convection terms might be treated explicitly without any CFL constraints, we still discretize them implicitly. For the 20mm test case, time steps $\delta t = 0.025\mathbf{s}$. For the 5mm test case, time steps $\delta t = 0.005\mathbf{s}$. Internal iterations for linearisation and for the projection method are set to ensure a decrease of oders of magnitude the residue. Practically, it requires up to 20 internal iterations at the beginning of the simulations (before the wall-jet impacts take place). This number of iterations decreases down to 3 iterations when the flow is more or less stationary.

VII. COMPARISONS BETWEEN NUMERICAL AND EXPERIMENTAL RESULTS

The 5mm case

We are comparing the simulation results and the experimental results at the location of the 10 sensors, for a time varying between 0 and 310**s** . Figure 5 shows that experimental and numerical results are in good agreement. Most of the results differ with less than 10 % of spreading, except for sensors 9 and 4 where numerical simulations underestimate helium concentrations by 20 %.

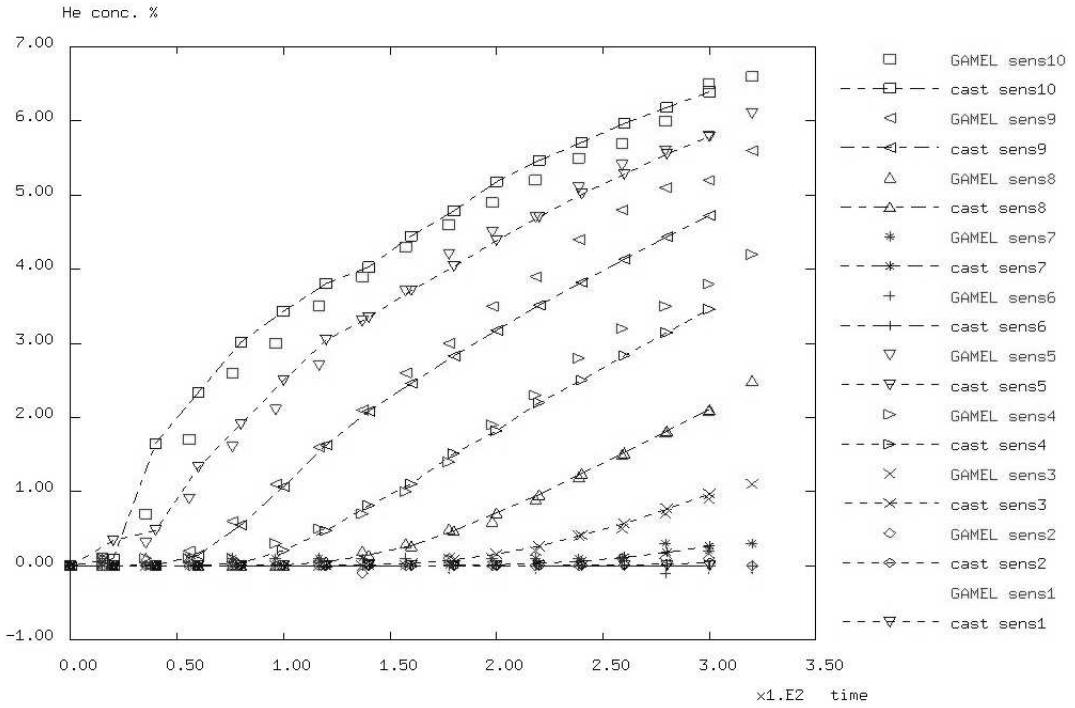

FIG. 5: Numerical versus experimental helium concentrations (by vol.) at the sensor locations with the 5mm nozzle. GAMEL refers to the experiments GAMELAN [4] and cast refers to cast3M calculations.

It appears that stratification is stronger than it should be. Experimental results show a small presence of an almost homogeneous layer at the top of the enclosure, which is not observed in the numerical simulations. In fact, we observe a larger variation of the numerically simulated concentrations at the top of the enclosure as in the experiments (sensors 10, 5 and 9, Figure 5). Nevertheless, a reversal vortex is indeed observed at the top of the enclosure in the numerical simulations, see Figure 6. The velocity field was rescaled by the square root of its norm for visualisation purposes. We suspect that a reason why an homogeneous layer is not observed on the numerically simulated concentration profiles may be due to smaller velocities than in the experiments or a smaller thickness. It is possible that our modified geometry is at the origin of the phenomenon.

The 1D distribution of the helium concentration is confirmed, both on previous Figure 5 where alternate results given by sensors 1 to 5 and sensors 6 to 10 fit in smoothly and on the helium concentration distribution given by numerical simulations at 306**s** , Figure 7.

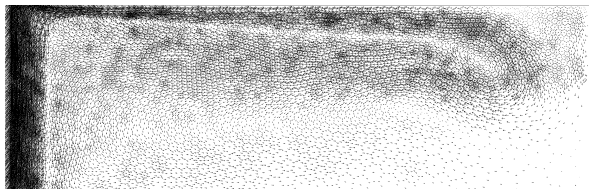

FIG. 6: Velocity field close up at the top of the enclosure with the 5mm nozzle.

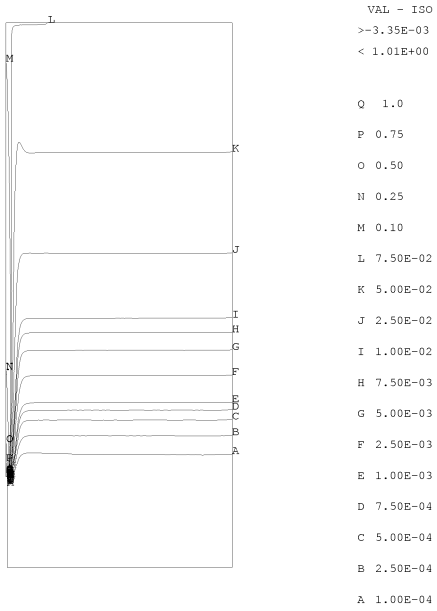

FIG. 7: Helium concentration at 306**s** in a cross section plan with the 5mm nozzle.

The 20mm case

We are also comparing the simulation results and the numerical results at the location of the 10 sensors, for a time varying between 0 and 1200**s** . We can observe, Figure 8, that experimental and numerical results are in acceptable agreement. Nevertheless, differences between simulated and experimental results are higher than with the 5mm case.

We observe a smaller simulated concentration at the top (sensors 10 and 5) than experimental measurements. Then, as we can see Figure 9, a larger stratification is observed on the numerical simulations results which leads to higher concentration than normal at the bottom of the enclosure and similar concentrations at the middle (sensor 6). The homogeneous layer is present at the top of the enclosure on the experimental data but is not observed in the numerical results. The main reason for this is probably due to the fact we have considered the flow as axisymmetric. We are not able to capture the experimentally observed (BOSS visualisation) oscillating patterns of the buoyant jet along the path from the injection to the top of the enclosure. This patterns are also theoretically expected, the Reynolds number in the jet being around 200 [13]. Numerical and experimental results are in better agreement with the 5mm nozzle, since these oscillations are

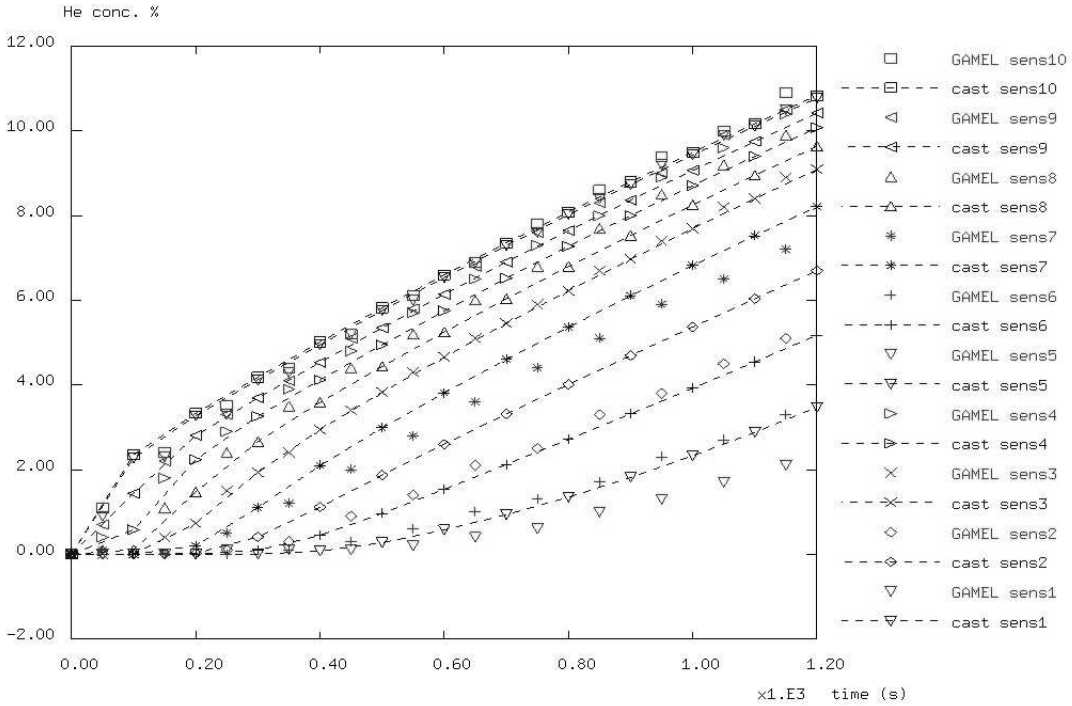

FIG. 8: Numerical versus experimental helium concentrations (by vol.) at the sensor locations with the 20mm nozzle.

decreasing with increasing Reynolds numbers. On the other hand, a reversal vortex is also observed at the top of the enclosure in the numerical simulations, see Figure 10. The 1D distribution of the helium concentration is also confirmed by the numerical concentration maps, see Figure 11.

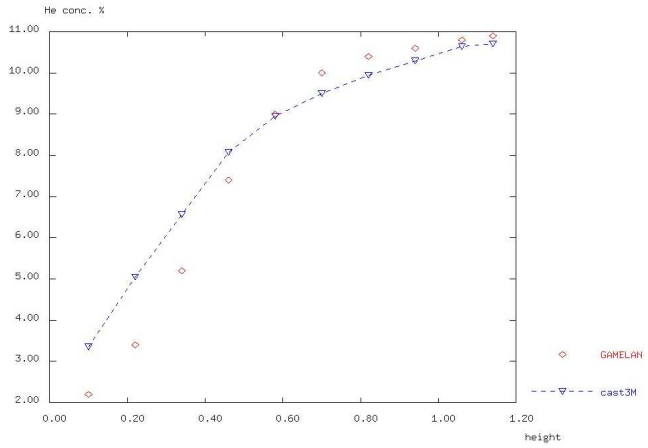

FIG. 9: Numerical versus experimental helium concentrations (by vol.) vertical profiles with the 20mm nozzle at 1200**s** .

We point out that the mass conservation has been checked for the numerical simulations and is satisfied at the computer's precision. When differences occur between simulated and measured concentrations, they just reflect that more mass is contained in the jet or in the layer located above the highest sensor (number 10).

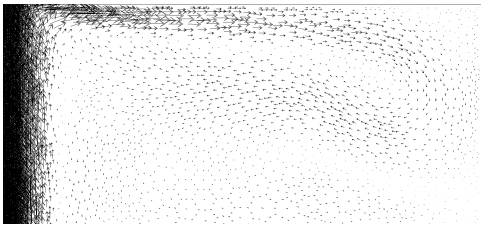

FIG. 10: Velocity field close up at the top of the enclosure.

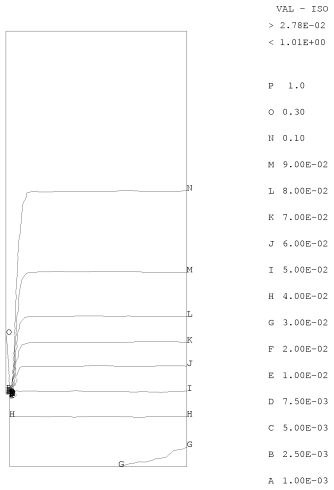

FIG. 11: Helium concentration at 1200**s** in a cross section plan with the 20mm nozzle.

VIII. DISCUSSIONS AND CONCLUDING REMARKS

We have produced a simplified numerical model to represent an almost cubic enclosure with a two dimensional axisymmetric geometry. Simplified incompressible conservation equations have been used with a Boussinesq approximation for the density variation. The simulations produced overall good results but with a larger helium concentration stratification than observed in the experiments.

Nevertheless, the main characteristics of helium distribution are found: the maximum concentration is obtained with less than 10% of difference compared to experiments, furthermore a reversal vortex is observed on the velocity fields and also on the helium concentrations vertical profiles. Results obtained with the 5mm injection nozzle are much closer to the experimental results, probably due to the fact that the jet is indeed axisymmetric, our simplifications being therefore better justified. At last, we observe almost a twice higher maximum of concentrations with the 5mm injections than with the 20mm injection, for almost the same helium injection flux. This result was also observed experimentally and is contradicting simple models predictions [2].

Our next goal is to use the numerically calculated velocity fields to have a better understanding of these differences. We also consider to run full 3D simulations, but still on a 3D cylinder to have a better fit between experimental and numerical results for highly buoyant flows.

IX. ACKNOWLEDGMENTS

This work has been supported by French Research National Agency (ANR) through Plan d'Action National sur l'Hydrogène et les piles à combustible program (project DIMITRHY n°ANR -08-PANH-006).

---

[1] W. D. Baines and J. S. Turner, *Turbulent buoyant convection from a source in a confined region*, J. Fluid Mech. **37**, 51 (1967).
[2] M. G. Worster and H. E. Huppert, *Time-dependant density profiles in a filling*, J. Fluid Mech. **132**, 457 (1983).
[3] P. F. Linden, G. F. Lane-Serff, and D. A. Smeed, *Emptying filling boxes : the fluid mechanics of natural ventilation*, J. Fluid Mech. **212**, 309 (1990).
[4] B. Cariteau, Rapport DM2S/SFME/LEEF RT/2010-016/A, CEA (2010).
[5] R. P. Cleaver, M. R. Marshall, and P. F. Linden, *The build-up of concentration within a single enclosed volume following a release of natural gas*, J. Hazardous Mater. **36**, 209 (1984).
[6] P. N. Papanicolaou and E. J. List, *Investigation of round vertical turbulent buoyant jets*, J. Fluid Mech. **195**, 341 (1969).
[7] J. Smagorinsky, *General circulation experiments with the primitive equations: 1. the basic experiments*, Mon. weather rv. **91(3)**, 99 (1963).
[8] Launder, *Turbulence*, Heat and Mass Transfer pp. 231–287 (1978).
[9] M. R. Swain, E. S. Grilliot, and M. Swain, *Experimental verification of a hydrogen risk assessment method*, Chemical Health and Safety pp. 28–32 (1999).
[10] I. Babùska, *The finite element method with lagrangian multipliers*, Numer. Math. **20**, 179 (1973).
[11] S. Badia and R. Codina, *Algebraic pressure segregation methods for the incompressible navier-stokes equations*, Archives of Computational Methods in Engineering **15**, 343 (2007).
[12] A. Ern and J.-L. Guermond, *Éléments finis: théorie, applications, mise en œuvre* (Springer, 2002).
[13] S. V. Patankar, *Numerical heat transfer and fluid flow* (Hemisphere, 1980).